Int. J. Multiphase Flow, Vol. 2, pp. 221–233. Pergamon/Elsevier, 1975. Printed in Great Britain.

TURBULENCE STRUCTURE OF AIR–WATER BUBBLY FLOW—I. MEASURING TECHNIQUES

AKIMI SERIZAWA
Institute of Atomic Energy, Kyoto University, Uji, Kyoto, Japan

and

ISAO KATAOKA and ITARU MICHIYOSHI
Department of Nuclear Engineering, Kyoto University, Sakyo-ku, Kyoto, Japan

(*Received* 1 *September* 1974)

Abstract—This paper, the first in a series describing our work on the turbulence structure of air–water bubbly flow, describes the principles of measurement and specially developed electronic instrumentation for determining various important local parameters, and the rates of turbulent transport of heat and bubbles in air–water two-phase bubbly flow. These instruments indicate the phase distribution, the bubble velocity and its spectrum, the water velocity and the turbulent intensity, and the turbulent dispersion coefficient of bubbles. Brief discussions are also presented on the accuracy of these techniques.

INTRODUCTION

In the study of two-phase flow there has been a strong need for instruments able to measure the detailed distributions of various local parameters including the distribution of the two phases, the bubble velocity and its spectrum, a fluctuating liquid velocity, bubble size distribution, bubble transit frequency, shear stress, and the turbulent transport characteristics of heat, momentum and bubbles. Though much effort has been spent (Hewitt 1972) two-phase flow instrumentation has not yet reached the point where all of the desired measurements can be made.

Of many local parameters, the void fraction is the most important quantity for engineering use, e.g. for the design of nuclear reactors, steam boilers, evaporating equipment, refrigerating equipment, etc. Accordingly, during the past 15 years the determination of the local void fraction has been emphasized. Due to the statistical nature of two-phase flow, all successful methods are based on either a length- or time-averaging concept. A gamma-ray traversing technique (Petrick 1958) belongs to the former, while an isokinetic sampling method (Gill *et al.* 1962; Schraub 1967; Shires *et al.* 1966), an electrical resistivity probe method (Neal 1963; Nassos 1963), a hot-film anemometer technique (Hsu *et al.* 1963, Delhaye 1968, 1969), and an optical-fiber probe method (Miller *et al.* 1969) are all of the latter kind. Among these methods, the electrical resistivity probe is best suited for the present work because of its easy usage and wide applicability. The principle of this method is described below.

To clarify the turbulence structure of two-phase flows, particularly of bubbly flow, an experimental determination of the velocity profiles of the two phases and the local void fraction profile is needed. However, it has been more difficult to measure accurately these quantities than the local void fraction. For measurement of the liquid velocity, the impact probe method was first proposed by Neal (1963). This method seems tenuous, and we cannot find any theoretical interpretation of the impact pressure in two-phase flow (Shires *et al.* 1966). The present authors (1973) and Kobayashi *et al.* (1973) have independently proposed a tracer technique for water velocity measurement. As a tracer, the former used salt water or hot water injected into the stream, whereas the latter used hot water generated by a special electronic circuit (thermal pulse generator). Recently, Delhaye (1969) proposed the hot-film anemometer technique. He treated the output signal of the anemometer probe, which fluctuates proportionally with the liquid velocity and phase change with a multichannel pulse height analyzer. With careful treatment and

time-consuming work in data reduction, this method gives accurate information about the time-average local liquid velocity and the turbulent intensity.

The bubble velocity distribution across the pipe was measured by Malnes (1966) in a steam–water system and also by Lackme (1967) in an air–water system by calculating the cross-correlation function between the output signals of two probe sensors. In calculating the cross-correlation function, Malnes used an analog computer, and Lackme used a correlator. The use of this cross-correlation technique is suitable for obtaining the local mean bubble velocity. (However, strictly speaking, this value is the most probable one, but is slightly different from the true mean velocity. This problem is discussed below.) A double-sensor probe method was also reported by Kitayama (1972) and Aoki *et al.* (1969). They measured the time lag between a pair of *START–STOP* signals of the probe with an electronic circuit and by photograph, respectively. Their treatments have a shortcoming in using averaging procedures or counting statistics for getting the mean bubble velocity, and therefore could not always give reliable information on the bubble velocity profile.

The mixing characteristics of the fluid are of great interest and importance in considering the mechanism of the turbulent transport process of transferable quantities. A considerable amount of knowledge has been obtained about the axial dispersion of the liquid in gas–bubble columns (e.g. Reith *et al.* 1968), but little information exists on turbulent transport properties of bubbles suspended in the liquid.

In the present study of the turbulence structure of upward air–water bubbly flow in a pipe, a new instrument is presented for measuring the local void fraction, the bubble impaction rate, the bubble velocity, and its spectrum. This instrument consists of a double-sensor probe (electrical resistivity probe), a newly developed electronic circuit, a digital counter and a multichannel analyzer. To clarify the usefulness and to examine the accuracy of the cross-correlation technique, we also used a correlator in bubble velocity measurement. Some comments are presented on the hot-film anemometer technique for measuring the liquid velocity and turbulent intensity. Last, we present new principles for measuring the turbulent dispersion coefficient of bubbles and the eddy diffusivity of heat by means of tracer techniques.

MEASURING SYSTEMS AND ACCURACY

In figures 1 and 2 are shown a block-diagram of the instrumentation and the electronic circuits developed for the present purposes.

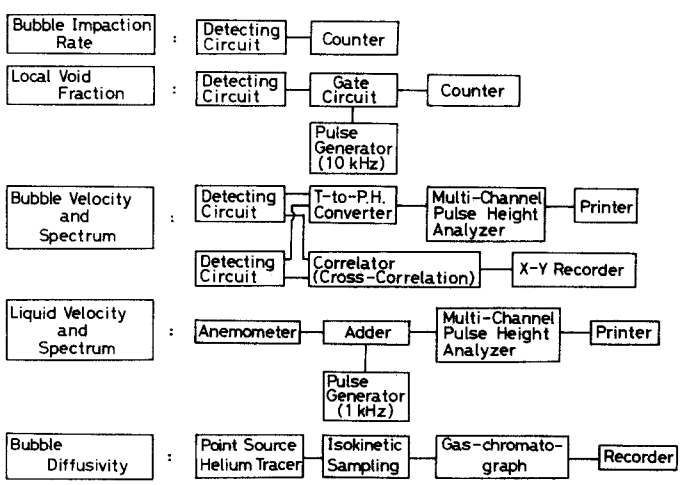

Figure 1. Block-diagram of the principles of measurements.

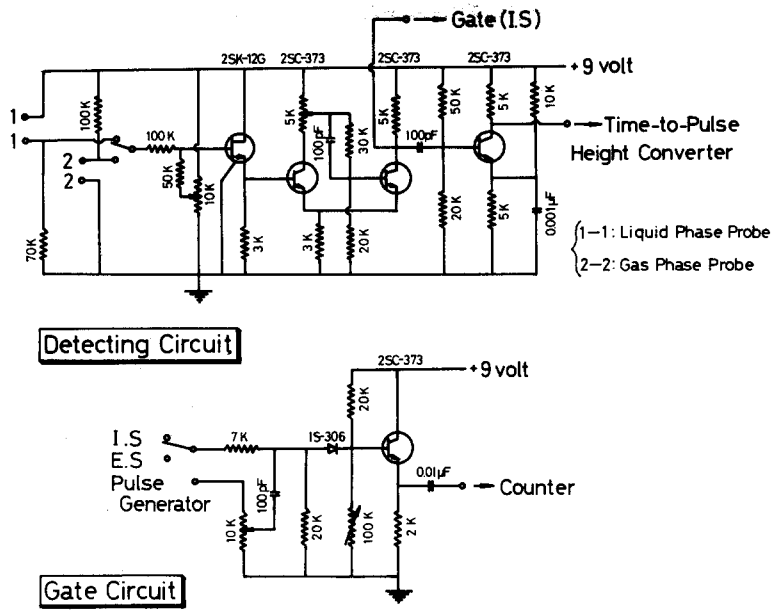

Figure 2. (a) Wiring-diagram of electronic circuit.

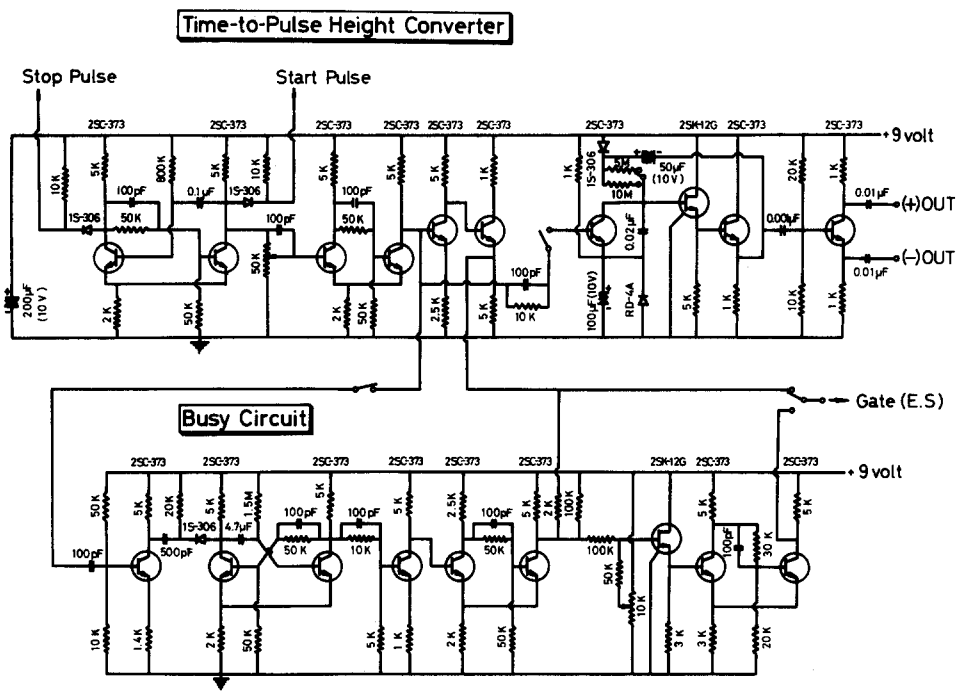

Figure 2. (b) Wiring-diagram of electronic circuit.

Local void fraction

The resistivity probe method is based on the difference in electrical resistivity between the liquid and the gas phases. This method was first proposed by Neal (1963) and by Akagawa (1963). But up to now, the ratio of the periods while the probe tip is in contact with gas phase to the total sampling time has not been proved theoretically to approximate the local void fraction. Recently, Iida (1972) and Serizawa (1974) have succeeded independently in solving this problem. It should be noted that the resistivity probe method, as well as other probe methods, is valid only in the case when the sampling time is sufficiently long to allow the statistical treatment of the bubbles. In the present experiment, the sampling time was 1 to 3 minutes. This is sufficiently long for good

counting statistics. The local void fraction $\alpha_{loc}(r)$ is given by

$$\alpha_{loc}(r) = \sum_i t_{gi}/T, \qquad [1]$$

where t_{gi} and T are the gas-contact period and total sampling time.

As shown in figure 3, the electrical resistivity probe consists of two identical sensors or needles, whose tips are about 5 mm apart from each other. Each needle is made of stainless steel wire of 0·2 mm dia, and is insulated electrically from the sheath except for its tip. The sensor which is located upstream is called the *START* probe, and the other the *STOP* probe. The change in resistance between the probe tip and the ground corresponding to the phase change is gradual for an air–water system, due to the poor wettability of the probe. Hence, the probe signal has to be altered to a square-wave response by a Schmitt trigger. The error associated with the effects of the probe geometry upon the bubble motion, the wettability effect, the bubble transfiguration and the decrease in bubble velocity is estimated to be less than 3%.

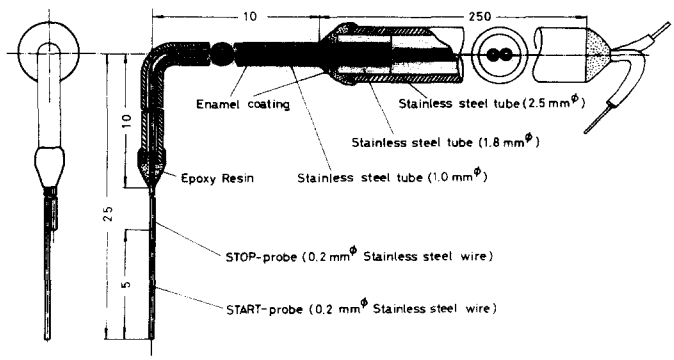

Figure 3. Double-sensor probe.

Bubble impaction rate

The bubble impaction rate was also measured by the resistivity probe method, utilizing only the *START* signal. Namely, the number of the modified square-wave signals from the *START* probe, which corresponds to the number of bubbles arriving at the measuring station for a given time duration, was counted by a digital counter.

Bubble velocity and its spectrum

Bubble velocity can be detected by the velocity of displacement of the interface between the gas and the liquid. When a bubble with a velocity V_b hits the *START* probe, a signal represented by the curve ⓐ is obtained as shown in figure 4. Presently, the same bubble hits the *STOP* probe (located a distance ΔZ downstream), and a signal (curve ⓐ′) similar to that from the *START* probe is obtained. The time lag between these two signals τ_0 is inversely proportional to the bubble velocity:

$$V_b = \Delta z/\tau_0. \qquad [2]$$

The time lag τ_0 of the travelling bubble can be deduced by the following two methods: one is the so-called cross-correlation technique and the other is the multichannel technique. The former method gives the average time lag of bubbles (in a strict sense, it is not "average" but the most probable time lag), whereas the latter gives the spectrum of the time lag for each bubble.

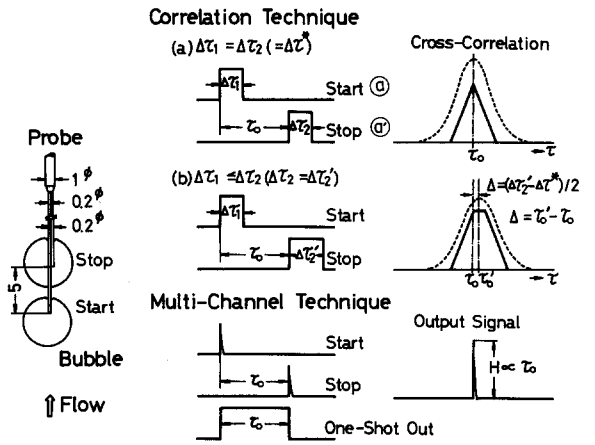

Figure 4. Correlative representation between cross-correlation and multichannel techniques.

(A) *Cross-correlation technique.* The cross-correlation function $F_{xy}(\tau)$ is:

$$F_{xy}(\tau) = \lim_{T\to\infty} \frac{1}{T} \int_0^T x(t-\tau)y(t)\,dt, \qquad [3]$$

where $x(t)$ and $y(t)$ are the *START* and *STOP* signals. A correlator (Model SAI-42, Signal Analysis Industries Corporation, U.S.A.) plotted $F_{xy}(\tau)$ as a function of the time lag τ via an X–Y recorder. From $F_{xy}(\tau)$, it is possible to find the most probable time lag τ_0 for bubbles to travel the distance from one probe to the other as a maximum point of $F_{xy}(\tau)$.

Let $x(t)$ and $y(t)$ be two ideal square-wave signals of the pulse width $\Delta\tau_1$ and $\Delta\tau_2$, respectively. Consider the cross-correlation function between $x(t)$ and $y(t)$. As shown in figure 4, two cases are encountered:

(a) $\Delta\tau_1 = \Delta\tau_2 (= \Delta\tau^*)$.

The time lag τ_{max}, which corresponds to the maximum value of the function $F_{xy}(\tau)$, is equal to τ_0.

(b) $\Delta\tau_1 \leq \Delta\tau_2 (= \Delta\tau_2')$.

In this case, τ_{max} is greater than τ_0 by $(\Delta\tau_2' - \Delta\tau^*)/2$. Experiments indicated that case (b) was more common than case (a), since bubbles were apt to encounter a larger hydraulic resistance when penetrating the *STOP* probe than when penetrating the *START* probe. This suggests that the bubble velocity measured by the corss-correlation technique tends to be a little lower than the actual velocity. An advantage of this method is its capability of prompt measurement (about 30 sec) and ease in data reduction.

(B) *Multichannel technique.* A time-to-pulse height converter shown in figure 2 was employed in order to get for each bubble a pulse proportional to the time lag τ_0 (denoted H in figure 4). This method gives information on the local "mean" bubble velocity and on the bubble velocity spectrum; however it requires time-consuming labor in data reduction. In the multichannel technique there exists a problem relating to a uniform statistical error which is independent of the flow variables. This error may result from the fact that one *STOP* signal is not always preceded by *START* signal caused by the same bubble. The following three cases may be encountered (figure 5):

(a) No other bubbles hit the *STOP* probe within the time duration between the *START* and *STOP* signals caused by the same bubble. This is the case for normal operation.

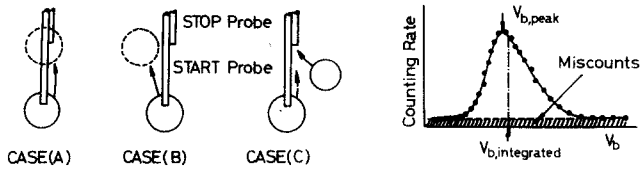

Figure 5. Probe configurations and bubble velocity histogram.

(b) A bubble, having penetrated the *START* probe, does not hit the *STOP* probe. In this case, the *START* signal produces a unique pulse as the output of the time-to-pulse height converter.

(c) Before a bubble, having penetrated the *START* probe, reaches the *STOP* probe another bubble hits the *STOP* probe.

The last two cases cause the miscounting. Since these cases can be assumed to occur statistically uniformly with respect to time, they function as a uniform background in the bubble velocity spectrum (figure 5). Hence, the ensemble-average bubble velocity is calculated by subtracting it from apparent bubble velocity spectrum. The bubble velocity $V_b(r)$ and standard deviation of bubble velocity spectrum s are given by

$$V_b(r) = \sum_i (N_i - N_{0i}) V_{bi}(r) / \sum_i (N_i - N_{0i}), \qquad [4]$$

$$s = \left[\sum_i (N_i - N_{0i}) \{V_b(r) - V_{bi}(r)\}^2 \Big/ \sum_i (N_i - N_{0i}) \right]^{1/2}; \qquad [5]$$

where N_i and N_{0i} are the total counting rate and the background component at V_{bi} in V_b vs N diagram.

Experimental results indicate that the average velocity of bubbles measured by the cross-correlation technique is about 5% smaller in bubbly flow than that measured by a multichannel technique (figure 6). Two reasons are possible for this difference. One has been already discussed with reference to figure 4. The alternative is related to the shape of bubble velocity spectrum. The results obtained by the multi-channel technique clearly indicate that the velocity spectrum of bubbles passing a certain point in the stream can be well approximated by a Poisson probability distribution function (e.g. figure 7 in the following paper). Also, it is seen in figure 5 that the peak velocity in the spectrum, $V_{b,peak}$, approximately equals the most probable velocity measured by the cross-correlation technique and is lower by 5 to 10% in bubbly flow, and

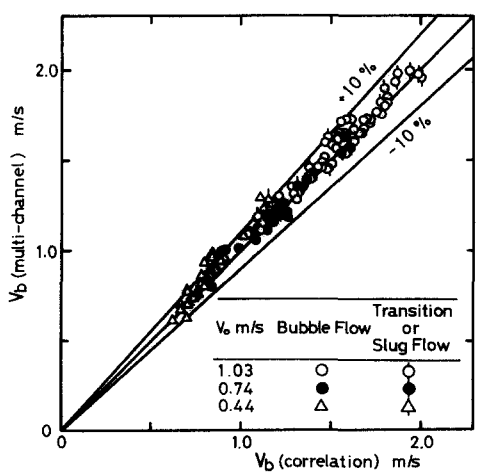

Figure 6. Comparison between bubble velocities measured by cross-correlation technique and by multichannel technique.

10 to 20% in transition and slug flows than the average (number-average) velocity of bubbles $V_{b,\text{integrated}}$.

Water velocity and its spectrum

Hot-film anemometry was used for this purpose. The electronic instrumentation consists of a hot-film probe, a constant-temperature anemometer (DISA 55D01), a linearizer (DISA 55D15), an auxiliary unit (DISA 55D25), a pulse generator (1 kHz), an adder, a biased amplifier (ORTEC Model 408), a 400-channel pulse height analyzer (VICTREEN PIP-400AA), and a digital printer. In all experimental runs, the overheating ratio of the hot-film probe (Thermo-Systems Inc. Model 1231) was 0·03 (Delhaye 1969). Prior to each experimental run, the anemometer was calibrated in upward water flow in the same test section vs a Pitot tube. According to Delhaye (1969) the average velocity of the liquid V_l and the longitudinal turbulent intensity $u'(=\sqrt{\overline{u^2}})$ are:

$$V_l = \sum_i V_{li}(N_i - N_{0i}) / \sum_i (N_i - N_{0i}), \qquad [6]$$

$$u' = \left[\sum_i (V_{li} - V_l)^2 (N_i - N_{0i}) / \sum_i (N_i - N_{0i}) \right]^{1/2}, \qquad [7]$$

where N_0 is the contribution by bubble passages to the N vs V_l histogram, and functions as a background in the calculating procedures (hatched part in figure 7).

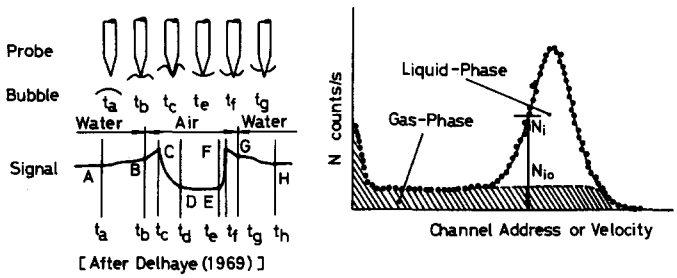

Figure 7. Passage of a single bubble past the conical hot-film probe and velocity histogram.

Hinze (1959) has pointed out in detail the limitations for applying the anemometer method to a flow where the relative turbulent intensity is large. When applying the hot-film anemometer technique to the present study of air–water two-phase bubbly flow, some questions arise in relation to the calibration procedure. Since we expect that the turbulent characteristics of air–water bubbly flow are different from those of single-phase water flow, the mechanism of heat transfer from the hot-film probe is different. However, inspecting our experimental results obtained by hot-film probe suggests that within the range of flow variables covered in the present work, the turbulent intensity in bubbly flow is the same order as in water flow (see figure 12 in the next paper in this series). Total liquid flow rate calculated by integrating the velocity profiles of the water measured by anemometry and the void fraction profiles measured by resistivity probe showed a good agreement with that measured directly by the turbine-flowmeter. Hence, the calibration of the anemometer obtained in water flow is considered valid also for bubbly flow whenever the temperature of the ambient fluid and the overheating ratio of the probe are kept constant.

Eddy diffusivity of heat

The radial eddy diffusivity of heat in air–water bubbly flow can be determined by measuring both radial and axial temperature distributions from a line heat source located perpendicular to

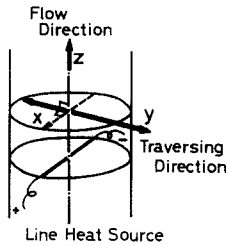

Figure 8. Coordinates system and heater arrangement.

the flow direction. Assuming radially independent diffusivity of heat, the diffusion equation similar to the equation of transient heat conduction in a solid can be applied (Serizawa 1974).

For a line heat source of infinite length and strength Q_0 per unit length along the x-axis located in the stream perpendicular to the flow direction (z-axis, figure 8), the initial conditions are

$$t = 0: \ \bar{\theta} - \bar{\theta}_0 = Q_0/c_p\rho_l \equiv Q^* \quad (\text{for } y = 0),$$

$$= 0 \qquad\qquad (\text{for } y \neq 0).$$

The solution is

$$\bar{\theta}(y, t) - \bar{\theta}_0 = \frac{Q^*}{2\pi \int_0^t 2\epsilon_H(t)\,dt} \exp\left[-\frac{y^2}{2\int_0^t 2\epsilon_H(t)\,dt}\right], \qquad [8]$$

where $\bar{\theta}_0$, the reference temperature of the fluid, is the temperature at a point far from the source. Equation [8] is derived assuming uniform radial distributions of local void fraction and velocities of the phases, and negligibly small molecular diffusion. This solution represents the temperature rise distribution in the plane $Z = \int_0^t V\,dt$, where V is given by

$$V = [\bar{V}_l\{1 - \bar{\alpha}_{loc}(S_{loc} - 1)\}]_{r=0}. \qquad [9]$$

The second term on the right hand side of [9] represents the effect of the backflow caused by the relative velocity between the phases. A bar denotes time-averaging, $\bar{V}_l$, $\bar{\alpha}_{loc}$, and S_{loc} are the time-average liquid velocity, the local void fraction, and the ratio between the velocities of the two phases, respectively. Then, the eddy diffusivity $\epsilon_H(t)$ is given by

$$\epsilon_H(t) = 1/2(d\overline{y_\theta^2}/dt), \qquad [10]$$

where

$$\overline{y_\theta^2} = \int_0^\infty \{\bar{\theta}(t,r) - \bar{\theta}_0\} r^2\,dr \Big/ \int_0^\infty \{\bar{\theta}(t, r) - \bar{\theta}_0\}\,dr. \qquad [11]$$

In the above equation, the lateral coordinate y is replaced by radius r.

Five chromel–alumel thermocouples of 0·65 mm in sheath diameter were utilized for measuring the radial and axial temperature distributions, and one for reference temperature which was located upstream of the line heat source. The line source was made of a chrome–nickel wire of 0·2 mm diameter, and it was heated by about 25 V d.c. (about 100 to 150 W) (figure 9).

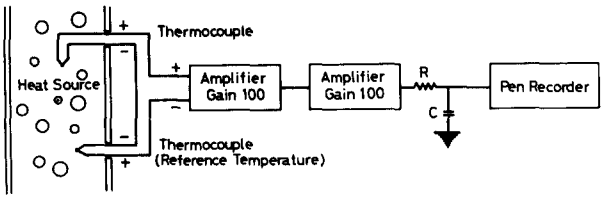

Figure 9. Instrumentation for measuring eddy diffusivity of heat.

Turbulent dispersion of bubbles

Assuming a homogeneous and isotropic turbulent flow field, the radially independent turbulent dispersion coefficient for bubble transport can be determined. For the case where good statistics are available for bubble counting, the bubble concentration distribution can be satisfactorily replaced by the bubble impaction rate distribution. This proof is subject to the following additional assumptions:

(1) Uniform bubble velocity in the radial direction.

(2) The mean diameter of bubbles at a certain point is independent of the radial position.

(3) The mean eccentricity between the probe tip and the bubble center is uniform in the radial direction.

The conservation of mass is applied to describe bubble transport in turbulent pipe flow similarly to Ginsberg (1971). For the case of no bubble sink or source in the flow field, the mass conservation of bubbles at a velocity V_b is

$$\frac{\partial C}{\partial t} = \phi(t)\frac{1}{r}\frac{\partial}{\partial r}\left(r\frac{\partial C}{\partial r}\right), \qquad [12]$$

where C and $\phi(t)$ are the mass concentration of bubbles and time-dependent turbulent dispersion coefficient of bubbles, respectively. For a point source of bubbles of strength S_0 at the origin of the coordinates, the solution to [12] is Gaussian in the case of no wall effects,

$$C(r,t) = \frac{S_0}{2\pi\int_0^t 2\phi(t)\,\mathrm{d}t}\exp\left[-\frac{r^2}{2\int_0^t 2\phi(t)\,\mathrm{d}t}\right]. \qquad [13]$$

In this case, the bubble dispersion coefficient $\phi(t)$ is

$$\phi(t) = 1/2(\mathrm{d}\overline{y(t)^2}/\mathrm{d}t), \qquad [14]$$

where the mean square of bubble displacement $\overline{y(t)^2}$ is given by

$$\overline{y(t)^2} = \int_0^\infty r^3 C(r,t)\,\mathrm{d}r \Big/ \int_0^\infty rC(r,t)\,\mathrm{d}r. \qquad [15]$$

The bubble concentration distribution data was obtained by an isokinetic sampling probe (figure 10). The probe diameter was small compared with the probable bubble diameter (about 4 mm). Hence within the range of our experiments, the instrument functions as a voidage probe (Shires *et al.* 1966).

The novelty of the present work is in using the isokinetic probe to obtain the turbulent dispersion coefficient of gas bubbles, by analyzing the mass concentration of tracer gas bubbles

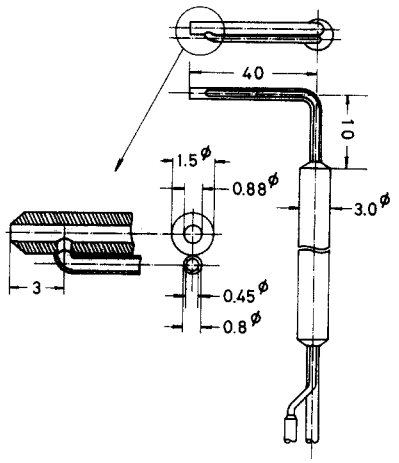

Figure 10. Isokinetic sampling probe.

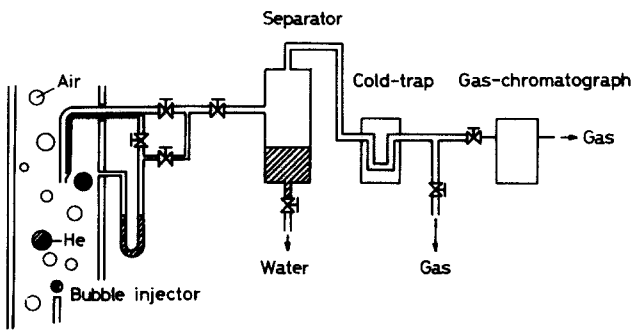

Figure 11. Instrumentation for measuring bubble dispersion.

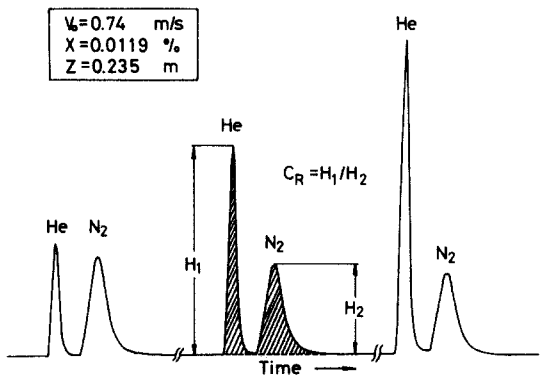

Figure 12. Typical records of the output signal of gas-chromatograph.

present in the sampled air–water mixture by means of a gas chromatograph. Helium tracer bubbles were injected into the stream of air–water mixture at constant volumetric flow rate from a bubble injector of 0·88 mm inside diameter located at the pipe center. Next, the gas phase including the helium and the air withdrawn was separated from the liquid by a separator and further dehydrated by a cold trap. Thereafter, the molar concentration of the helium involved per unit volume of the withdrawn and dehydrated gas was analyzed by a gas chromatograph (figure 11). Argon was used as a carrier gas to increase the resolution of the instrument. The output voltage of the instrument was recorded by a pen recorder. Typical results are demonstrated in figure 12 for different radial positions. The tracer gas bubbles are clearly discriminated from the air bubbles. By reading the peak values of the output for the helium and the nitrogen, we can easily get an indication of the helium mass concentration in two-phase flow in the following manner†.

Let C_R and C'_R be the apparent and the true molar ratio between the helium gas and the nitrogen in unit volume of the withdrawn mixture of air and helium, respectively (figure 12). Then

$$C'_R = k_1 C_R, \tag{16}$$

where k_1 is a correction factor for the difference in thermal conductivity of the helium and that of the nitrogen for a given bridge current and a given carrier gas. Assume $C'_R \ll M_{N_2}/M_{He}$, then the mass concentration of the helium contained within unit volume of the gas phase of air–water mixture C_g can be approximated by

$$C_g = k_2 C'_R (M_{He}/M_{N_2}) \equiv k C_R, \tag{17}$$

$$k = k_1 k_2 (M_{He}/M_{N_2}), \tag{18}$$

where M_{He} and M_{N_2} are the molecular weights of the helium and the nitrogen, respectively, and k_2 is the mass concentration of the nitrogen per unit volume of the air at system temperature and pressure. Provided the helium flow rate has no influence on the local flow condition of air–water bubbly flow, the local mass concentration of the helium involved within unit volume of air–water mixture $C(r)$ can be ultimately expressed as

$$\begin{aligned} C(r) &= C_g(r)\alpha_{loc}(r) \\ &= kC_R(r)\alpha_{loc}(r), \end{aligned} \tag{19}$$

or

$$\frac{C(r)}{C(0)} = \{C_R(r)/C_R(0)\}\{\alpha_{loc}(r)/\alpha_{loc}(0)\}. \tag{20}$$

Then, the turbulent dispersion coefficient of gas bubbles (in a strict sense, that of helium bubbles) can be deduced according to [14] and [15] from the experimental radial profiles of the relative mass concentration of the helium $C(r)/C(0)$ measured at several axial positions downstream of the bubble injector.

†Strictly speaking, the integrated values of the output signals corresponding to the helium and the nitrogen (hatched parts in figure 12) should be applied instead of their peak values.

REFERENCES

AKAGAWA, K. 1963 A study on fluctuating characteristics of the void fraction in gas–liquid two-phase flow. *Trans. Japan Soc. Mech. Engrs* **29**, 924–931.

AOKI, S., INOUE, A. & YAEGASHI, H. 1969 The local void fraction and velocities of the phases in two-phase bubbly flow in a vertical tube, *Proc. 6th Japan Heat Transfer Symp.* 241–244.

DELHAYE, J. M. 1968 Measurement of the Local Void Fraction in Two-Phase Air–Water Flow with a Hot-Film Anemometer. *CEA-R*-3465.

DELHAYE, J. M. 1969 Hot-film anemometry in two-phase flow. *Proc. 11th Nat. ASME/AIChE Heat Transfer Conf. on Two-Phase Flow Instrumentation*, Minneapolis, Minnesota, 58–69.

GILL, L. E., HEWITT, G. F. & HITCHEN, J. W. 1962 Sampling Probe Studies of the Gas Core in Annular Two-Phase Flow. Part I. The Effect of Length on Phase Velocity Distribution. AERE-R-3954.

GINSBERG, T. 1971 Droplet Transport in Turbulent Pipe Flow. ANL-7694.

HEWITT, G. F. 1972 The role of experiments in two-phase systems with particular reference to measurement techniques. *Progress in Heat and Mass Transfer* **6**, (Edited by HETSRONI, G., SIDEMAN, S. & HARTNETT, J. P.) pp. 295–343. Pergamon.

HINZE, J. O. 1959 *Turbulence.* McGraw-Hill.

HSU, Y. Y., SIMON, F. F. & GRAHAM, R. W. 1963 Application of hot-wire anemometry for two-phase flow measurements such as void fraction and slip velocity. *Proc. A.S.M.E. Winter Meeting*, Philadelphia.

IIDA, Y. 1972 Study on local void fraction, *J. At. Energy Soc. Japan* **14**, 337–339.

KITAYAMA, Y. 1972 Digital void velocimeter, *J. Nucl. Sci. Technol.* **9**, 613–617.

KOBAYASHI, K. & IRINO, Y. 1973 Phase velocities and slip ratios in gas/liquid two-phase flow. *Proc. 10th Japan Heat Transfer Symp.*, 41–44.

LACKME, C. 1967 Structure et Cinematique des Ecoulements Diphasiques a Bulles. CEA-R-3203.

MALNES, D. 1966 Slip Ratios and Friction Factors in the Bubble Flow Regime in Vertical Tubes. KR-110.

MILLER, N. & METCHIE, R. E. 1969 The development of a universal probe for measurement of local voidage in liquid/gas two-phase flow systems. *Proc. 11th Nat. ASME/AIChE Heat Transfer Conf. on Two-Phase Flow Instrumentation*, Minneapolis, Minnesota, pp. 82–88.

NASSOS, P. G. 1963 Development of an Electrical Resistivity Probe for Void Fraction Measurements in Air/Water Flow. ANL-6738.

NEAL, L. G. 1963 Local Parameters in Cocurrent Mercury–Nitrogen Flow. ANL-6625.

PETRICK, M. 1958 Two-Phase Air–Water Flow Phenomena. ANL-5787.

REITH, T., RENKEN, S. & ISRAEL, B. A. 1968 Gas hold-up and axial mixing in the fluid phase of bubble columns, *Chem. Engng Sci.* **23**, 619–629.

SCHRAUB, F.A. 1967 Isokinetic Sampling probe Technique Applied to Two-Component Two-Phase Flow, ASME Paper 67-WA/FE 28.

SERIZAWA, A., KATAOKA, I. & MICHIYOSHI, I. 1973 Turbulent structure of air–water bubbly flow (I) & (II). *Proc.* 1973 *Ann. Meet. At. Energy Soc. Japan.*

SERIZAWA, A. 1974 Fluid-Dynamic Characteristics of Two-Phase Flow. Doctoral Thesis, Kyoto University.

SHIRES, G. L. & RILEY, P. J. 1966 The Measurement of Radial Voidage Distribution in Two-Phase Flow by Isokinetic Sampling. AEEW-M650.

Auszug—Dieser Artikel ist der erste einer Reihe, die ueber unsere Untersuchungen der Turbulenzstruktur von Luft-Wasser-Zweiphasenstroemungen berichtet. Er beschreibt Grundzuege und eigens entwickelte Instrumentierung fuer die Messung wichtiger oertlicher Parameter, und turbulenter Transportgeschwindigkeiten von Waerme und Blasen in Zweiphasenstroemung von Luftblasen und Wasser. Die Instrumente zeigen die Phasenverteilung, die Blasengeschwindigkeit und ihr Spektrum, die Wassergeschwindigkeit und Turbulenzstaerke, sowie den turbulenten Dispersionskoeffizienten der Blasen an. Die mit dieser Technik erzielte Genauigkeit wird eroertert.

Резтоме—Настоящая статья, первая из серии, описывающих нашу работу в области турбулентной структуры водо-воздушного пузырькового течения, описывает принципы измерения и электронное оборудование, при способленное для определения важных изменяющихся местных параметров, а также скоростей турбулентного переноса тепла и пузырьков в водо-воздушном двуфазном пузырьковом потоке. Упомянутые инструменты указывают фазовое распределение, скоросуь пузырьков и их спектр, скорость воды и степень турбулентности, коэффициент турбулентного рассеяния пузырьков. Представлено также краткое обсуждение точности этих методов.